Published in final edited form as:
J Cell Sci. 2006 December 15; 119(Pt 24): 5124–5136. doi:10.1242/jcs.03292.

Multiple Controls Regulate Nucleostemin Partitioning Between Nucleolus and Nucleoplasm

Lingjun Meng[1], **Hiroaki Yasumoto**[1], and **Robert Y.L. Tsai**[1,*]

[1] Center for Cancer and Stem Cell Biology, Alkek Institute of Biosciences and Technology, Texas A&M Health Science Center, Houston, Texas 77030-3303, USA

Summary

Nucleostemin plays an essential role in maintaining the continuous proliferation of stem cells and cancer cells. The movement of nucleostemin between the nucleolus and the nucleoplasm provides a dynamic way to partition the nucleostemin protein between these two compartments. Here, we showed that nucleostemin contained two nucleolus-targeting regions, the basic and the GTP-binding domains, which exhibited a short and a long nucleolar retention time, respectively. In a GTP-unbound state, the nucleolus-targeting activity of nucleostemin was blocked by a mechanism that trapped its intermediate domain in the nucleoplasm. A nucleostemin-interacting protein, RSL1D1, was identified that contained a ribosomal L1-domain, co-resided with nucleostemin in the same subnucleolar compartment non-identical to the B23 and fibrillarin distributions, and displayed a longer nucleolar residence time than nucleostemin. RSL1D1 interacted with both the basic and the GTP-binding domains of nucleostemin through a non-nucleolus-targeting region. Overexpression of the nucleolus-targeting domain of RSL1D1 alone dispersed the nucleolar nucleostemin. Loss of RSL1D1 expression reduced the compartmental size and amount of nucleostemin in the nucleolus. This work reveals that the partitioning of nucleostemin employs complex mechanisms involving both nucleolar and nucleoplasmic components, and provides insight into the post-translational regulation of its activity.

Keywords

Nucleolus; Nucleoplasmic; Nucleostemin; Retention; RSL1D1; Stem cell

Introduction

The nucleolus is a subnuclear compartment organized around the tandem repeats of ribosomal DNAs. It has become evident that the nucleolus is a very dynamic organelle. All nucleolar components are engaged in complex movements (Andersen et al., 2005; Olson and Dundr, 2005). Most, if not all, nucleolar proteins shuttle between the nucleolus and the nucleoplasm at a relatively fast pace (Andersen et al., 2005; Chen and Huang, 2001; Dundr et al., 2000; Phair and Misteli, 2000; Tsai and McKay, 2005). Several nucleoplasmic proteins, such as p53 (Rubbi and Milner, 2000), telomerase reverse transcriptase (TERT) (Wong et al., 2002), the murine double minute protein (MDM2) (Weber et al., 1999), and the von Hippel-Lindau tumor suppressor protein (Mekhail et al., 2004; Mekhail et al., 2005), have been shown to associate with the nucleolar structure under physiological or pathological conditions, suggesting that it may serve as a form of subcellular machinery to

*To whom correspondence should be addressed to: R.Y.L. Tsai, 2121 W Holcombe Blvd, Houston, TX 77030-3303, (O) 713-677-7690, (Fax) 713-677-7512, rtsai@ibt.tamhsc.edu.

activate or inactivate proteins that may not always reside in it. Compartmentalization provides a fast and energy-conserving mechanism to modulate protein activities without changing their expression levels. The movement of nuclear proteins in and out of the nucleolus allows cells to respond to a variety of environmental stimuli in a fast and dynamic fashion (Carmo-Fonseca et al., 2000; Tsai, 2004).

The complexity of the molecular devices controlling the protein flux through the nucleolus is manifested in many aspects. Unlike proteins that travel to membrane-bound organelles, most nucleolar proteins do not share a consensus targeting sequence, and their nucleolar localization signals (NoLS) often overlap with the nuclear localization signals (NLS) (Martel et al., 2006; Reed et al., 2006; Sheng et al., 2004; You et al., 2005). Within the nucleolus, distinct subdomains can be identified by their electron dense properties and by the distribution of proteins or ribosomal RNAs (Politz et al., 2002; Politz et al., 2005). In addition to their nucleolar-nucleoplasmic shuttling behavior, some nucleolar proteins may temporally associate with other subnuclear organelles, such as the Cajal body, paraspeckles, and the promyelocytic leukemia nuclear body (Bernardi et al., 2004; Fox et al., 2002; Sleeman et al., 2003). The dynamics of nucleolar proteins can be further modified by environmental signals, such as the pH (Mekhail et al., 2004) and the intracellular GTP level (Tsai and McKay, 2005). It remains unclear why and how these proteins move so rapidly between different nuclear compartments. Understanding the mechanisms underlying this process may provide insight into the regulation of nucleolar functions in protein synthesis, posttranscriptional modification of RNAs, cell-cycle progression, and stress response (Pederson, 1998; Rubbi and Milner, 2003).

The dynamic movement of a nucleolar protein nucleostemin (NS) is controlled by a GTP-driven cycle (Misteli, 2005; Tsai and McKay, 2005). NS is highly enriched in the embryonic, mesenchymal, and neural stem cells, and several types of human cancers (Baddoo et al., 2003; Liu et al., 2004; Tsai and McKay, 2002). It enters the nucleolus in a GTP-bound form, mediated in part by its basic (B)-domain. When NS is in the GTP-unbound state, its nucleolar targeting ability is suppressed by the intermediate (I)-domain (Tsai and McKay, 2005). The GTP-binding capability of NS regulates its shuttling in and out of the nucleolus, and, given its function in maintaining the proliferation of stem cells and cancer cells, may be used to transduce extracellular signals into the mitotic state of these cells in a fast and reversible manner. In this study, we attempted to dissect the protein(s) and structural components that regulated the compartmentalization of NS. We showed that the nucleolar localization of NS was mediated by its B- and GTP-binding (G)-domains, which interacted with a ribosomal L1-domain-containing gene, RSL1D1, belonging to the L1p/L10e family. RSL1D1 co-localized with NS in the same subnucleolar domain and affected the nucleolar distribution of NS in the mutant overexpression and siRNA knockdown paradigms. Conversely, the movement of NS to the nucleolus was gated by a GTP-controlled mechanism that used the I-domain as a nucleoplasmic anchor. Together, these mechanisms determined the partitioning of NS between the nucleolus and the nucleoplasm.

Results

NS contained two nucleolar localization regions

Previously, we showed that B-domain deletion (NSdB) or Gly 256-to-Val mutation (G256V) could diminish the nucleolar localization of NS, and a combination of both (dB(G256V)) completely excluded it from the nucleolus (Tsai and McKay, 2005). To test whether the G-domain was sufficient to mediate nucleolar localization by itself, NS mutants containing the B-, G-, or both domains were examined for their distribution in U2OS cells (Fig. 1A and B). Our results showed that the B- and the G-domain proteins were predominantly localized to the nucleolus (Fig. 1B, B and nlsG). When both domains were

present, their nucleolar signal intensities relative to the nucleoplasmic intensities (N/P) appeared stronger than those of the B- and the G-domain alone (N/P values: NS, 3.0; NSdA, 3.2; B, 2.0; G, 1.9). To decide whether GTP-binding regulated the nucleolar localization of the G-domain, we made a mutation on the conserved Gly 256 residue in the nlsG mutant (nlsG(256)), showing that this double mutant remained in the nucleolus. However, if the I-domain was included, G256V mutation could disrupt the nucleolar distribution of the GI-domain (nlsGI(256)). In order to transport mutant proteins without NLS into the nucleus, a SV40 NLS (PKKKRKV) was engineered at the amino terminus of the G and GI mutants. This SV40 NLS did not display any nucleolar localization capability by itself when fused to a cytoplasmic hydrolase protein (nlsHd3). These data demonstrate that both the B- and the G-domain possess nucleolus-targeting activities. The nucleolar localization of the G-domain alone does not require GTP-binding, but is gated by the I-domain in a GTP-dependent manner.

Long retention of NS in the nucleolus was mediated by its G-domain

Because the nucleolar residence time of the B-domain is much shorter than that of the full-length NS (Tsai and McKay, 2005), the G-domain may mediate the long retention of NS in the nucleolus. We confirmed this idea by the FRAP (fluorescence recovery after photobleaching) approach, which showed that the nucleolar retention time of the GI-domain was longer than that of the B-domain or the full-length NS (Fig. 1C1). The difference in FRAP between the GI-domain and the full-length NS could be attributed to the acidic domain (A) deletion because the GI-domain exhibited the same recovery kinetics as the NSdA mutant during the first 20 seconds after photobleaching (Fig. 1C2, 1C3). Thirty seconds after photobleaching, the GI-domain appeared to recover more fluorescence signals in the nucleolus than NSdA did. In these experiments, we included the I-domain because a deletion of this region prolonged the FRAP recovery time significantly and often caused cell death (Tsai and McKay, 2005). Because the I-domain has no nucleolar localization activity, we conclude that the G-domain is responsible for the long nucleolar retention of NS.

A B- and G-domain-independent mechanism retained NS in the nucleoplasm

The I-domain might block the nucleolar localization of the GTP-unbound NS by masking its nucleolus-targeting regions or by a B- and G-domain-independent nucleoplasmic-retaining mechanism. To determine which of the two mechanisms was used by NS, we first examined whether the I-domain could interact with the B- or G-domain. Using affinity binding assays, we showed that glutathione S-transferase (GST) fusion of the I-domain was unable to bind any of the B- or G-domain-containing mutants, regardless of their GTP-binding states (Fig. S1 in supplemental data). To determine if the nucleoplasmic-retaining activity of the I-domain depended on the B- or G-domain, we tethered another nucleolar protein B23/nucleophosmin (B23) with an I-domain fragment at its amino (N)-terminus (myc-I-B23, Fig. 2A1) or carboxyl (C)-terminus (B23-I-HA, Fig. 2B1). Compared to the wild-type B23 protein, the presence of the I-domain significantly increased the nucleoplasmic portion of B23. This phenotype was I-domain-dependent, and not caused by the fusion *per se*, since B23 proteins tagged with the myc (Fig. 2A2) or HA epitope (Fig. 2B2), or the green fluorescent protein (GFP, 239 residues versus 176 residues in the I-domain, Fig. 2A3 and 2B3) at either the N- or the C-terminus displayed a wild-type B23 distribution. To further support these findings, we created I-domain fusions of three ribosomal proteins, L5, L11, and L23, showing that the I-domain could shift these proteins from a nucleolar-predominant distribution to a nucleoplasmic distribution (Fig. 2C, D, E). These results demonstrate that the I-domain possesses a B- and G-domain-independent activity that retains NS in the nucleoplasm.

Identification of a NS-interacting protein, RSL1D1

To identify proteins that might be involved in the nucleolar or nucleoplasmic retention of NS, a yeast two-hybrid screen was set up where a GAL4 DNA binding-domain fusion of the GI-domain was used to screen a mouse embryonic day 7-cDNA library for potential binding proteins. From a total of 5.6 million clones screened, two positive ones were isolated. They encoded an in-frame full-length cDNA of a ribosomal L1-like domain-containing gene RSL1D1 (NM_025546.1) (Fig. 3A). The biochemical interaction between NS and RSL1D1 was shown by affinity binding assays in which the HA-tagged NS or RSL1D1 could be specifically retained by agarose-bound GST fusions of RSL1D1 (Fig. 3B1) or NS (Fig. 3B2), respectively, but not by the GST backbone protein. To confirm the interaction between NS and RSL1D1 in vivo, HEK293 cells were transfected with both HA-tagged NS and myc-tagged RSL1D1 expression plasmids for coimmunoprecipitation. Our results showed that NS could be co-purified with RSL1D1 by anti-myc antibody, but not by mouse IgG (Fig. 3C, 1st row). Similarly, RSL1D1 could be detected in the NS protein complex precipitated by anti-HA antibody (3rd row). Finally, we demonstrated that endogenous NS in HEK293 cells and myc-tagged RSL1D1 could be co-purified in the same protein complexes precipitated by anti-NS antiserum (Fig. 3D, left panel) or by anti-myc antibody (right panel), but not by the control preimmune serum or mouse IgG. These results show that NS and RSL1D1 can form a protein complex both in vitro and in vivo.

RSL1D1 co-localized with NS in the same subnucleolar compartments non-identical to the B23 and fibrillarin distributions

To address if the interaction between NS and RSL1D1 was physiologically relevant, we first characterized the RSL1D1 expression during embryogenesis and in the adult tissues. Developmental Northern blots showed that the RSL1D1 message was abundantly expressed in the E10.5 and E12.5 embryos and decreased after E12.5. This expression window overlapped with that of NS (Fig. 4A). In adult mice, RSL1D1 was most highly expressed in the testis, followed by the muscle and eye. Other tissues expressed RSL1D1 at a low level (Fig. 4B). These results show that the expression pattern of RSL1D1 coincides with that of NS in the early embryos and in the adult testis (Tsai and McKay, 2002), and that RSL1D1 is more widely expressed than NS.

The subcellular distribution of RSL1D1 and NS was determined in U2OS cells by high-resolution confocal analyses. Our results showed that NS was non-uniformly distributed within the nucleolus (Fig. 4C1 and 4C2). To a great extent, the RSL1D1 signal, detected by a myc epitope or GFP tag, co-localized with NS (Fig. 4C3 and Fig. S2A in supplemental data). This distribution pattern was not identical to that of B23, which was less in the center and more in the periphery of the nucleolus (Fig. 4D and Fig. S2B in supplemental data). Conversely, the fibrillarin protein resided in small domains within the nucleolus that were low in the NS and RSL1D1 signals (Fig. 4E and Fig. S2C in supplemental data). These colocalization data provide a physiological basis for the NS-RSL1D1 interaction, and suggest that the nucleolar localization of NS and RSL1D1 may be co-dependent.

Nucleolar retention time of RSL1D1 was longer than that of full-length NS

Next, we used FRAP experiments to determine the nucleolar residence time of RSL1D1. A GFP-fusion of RSL1D1 was expressed in CHO cells. A FRAP paradigm was designed where a circle of 1um in diameter within the nucleolus was bleached (Fig. 5A, arrows), and the fluorescence recovery in the bleached area was recorded for 31.6 seconds (Fig. 5B). Our results showed that 5 seconds after photobleaching, the fluorescence recovery of RSL1D1 reached only 72.8% of the prebleached level, compared to the 80.9% recovery of NS (Fig.

5C). The FRAP recovery rate of RSL1D1 continued to lag behind that of NS throughout the 31.6-second recording period ($p<0.001$, n=20).

The NS-RSL1D1 interaction was mediated by the B- and G-domains of NS

To address if the NS-RSL1D1 interaction was related to the nucleolus-targeting activity of NS, we investigated which domains of NS were required for this interaction using a panel of truncated NS mutants (Fig. 6A). Affinity binding assays demonstrated that deletion of any single B-, C-, G-, I- or A-domain did not affect the NS binding to RSL1D1, indicating that multiple regions were involved (Fig. 6B). Using complex deletion mutants, we showed that RSL1D1 was able to interact with both the BC- and the GI-domain individually, but very little or not at all with the G-, IA-, or GI(256) mutants (Fig. 6C). The RSL1D1-binding domain of NS was further defined to the B-region of the BC-domain (Fig. 6D1) and to the GI1-region of the GI-domain, consisting of the G-domain plus the N-terminal 73 residues of the I-domain (Fig. 6D2). Finally, we confirmed that the B- and G-domains were the major binding interfaces for RSL1D1. A double deletion of these two domains (NSdBG) completely abolished the binding between NS and RSL1D1, whereas a double deletion of the C- and I-domains (NSdCI) had no effect on their interaction (Fig. 6D2). These results demonstrate that the RSL1D1-interacting and nucleolus-targeting domains of NS are the same.

Separate domains of RSL1D1 mediated its nucleolus-targeting and NS-binding activities

RSL1D1 contained an L1 domain (amino acid (a.a.) 150–254), a coiled-coil domain (a.a. 270–316), and three predicted NLS (Fig. 7A). To determine whether the NS-interacting domain of RSL1D1 overlapped with its nucleolar localization domain, we examined the NS-binding abilities and distribution patterns of RSL1D1 truncated mutants (Fig. 7A). Affinity binding assays showed that GST fusions of the BC- and the GI-domain could specifically retain the C-terminal half of RSL1D1 (255–452), but not the N-terminal half mutant (1–254), which included the L1-domain (Fig. 7B). We further defined the NS-interacting domain of RSL1D1 to its last 136 amino acids without the coiled-coil domain (317–452). The distribution patterns of different RSL1D1 domains in relation to NS were determined by double-labeled immunofluorescence (Fig. 7C-L). The 150–316 region of RSL1D1, which contained the L1-domain, the coiled-coil domain, and one NLS, was localized in the nucleolus (Fig. 7C). The 1–149 region by itself was distributed in the cytoplasm (Fig. 7D). When engineered with a SV40 NLS, a portion of it could enter the nucleolus (Fig. 7E). The NS-interacting 317–452 domain was diffusely localized in the nucleus (Fig. 7F), and, in some cells, displayed a slightly higher intensity in the nucleus than in the nucleoplasm (Fig. 7G). Further dissection of the nucleolus-targeting 150–316 region revealed that without a NLS, the L1 domain (150–254) was trapped mostly in the cytoplasm. Only a small portion of it was located around the nucleolus (Fig. 7H). When tagged with a SV40 NLS, the L1 domain (nlsL1) was able to enter the nucleolus (Fig. 7I). Notably, the nucleolar signal of NS was either diminished or absent in many cells expressing this nlsL1 mutant (Fig. 7J, bottom panel). The coiled-coil domain (255–316) exhibited a diffuse nuclear distribution similar to that of the 317–452 region (Fig. 7K). Finally, except for the nlsL1 construct, neither the mutants nor the wild-type RSL1D1 (Fig. 7L) appeared to affect the distribution of endogenous NS (Fig. 7C-L, bottom panels). These data demonstrate that the NS-interacting domain of RSL1D1 contributes little to its nucleolar localization. Instead, the nucleolar distribution of RSL1D1 is mediated mostly by the L1-domain and partially by the 1–149 region, neither of which binds NS.

Overexpression of nlsL1 reduced the amount of NS in the nucleolus

The nlsL1 mutant was localized in the nucleolus, but lacked the ability to bind NS. Compared to non-transfected cells, overexpression of this mutant distinctively reduced the amount of NS in the nucleolus (Fig. 8A1). Despite its reduced intensity, the distribution pattern of the remaining NS signal in those cells resembled the NS distribution in non-transfected cells (Fig. 8A2). In some cells, the NS signals were scattered around the nlsL1 signals (Fig. 8B), indicating that overexpression of this mutant could lead to either a disruption of the nucleolar structure or a displacement of NS from its original compartment. To determine whether nlsL1 disrupted nucleolar organization, we examined its effect on the distributions of fibrillarin and B23, which were involved in pre-ribosomal RNA processing and ribosome maturation, respectively. Judging from the signal intensities and distribution patterns, neither fibrillarin (Fig. 8C) nor B23 (Fig. 8D) was affected by nlsL1 overexpression. These results show that nlsL1 may function as a dominant negative regulator for the nucleolar distribution of NS.

Partial loss of RSL1D1 expression decreased the nucleolar distribution of NS

Because the RSL1D1-interacting domains of NS coincided with nucleolar localization regions, but the NS-interacting domain and the nucleolus-targeting domain of RSL1D1 were distinctively separated, we reasoned that the nucleolar distribution of NS might be secondary to that of RSL1D1. To test this idea, we knocked down the expression of RSL1D1 using the small RNA interference (siRNA) approach and examined the distribution of NS. Compared to the control siRNA (siNEG) knockdown samples, RSL1D1-specific siRNA (siRSL1D1) treatment reduced the RSL1D1 expression by 73% at the RNA level and 43% at the protein level, but did not affect the total protein level of NS (Fig. 9A). siRSL1D1-treated cells showed a mild but significant decrease in the nucleolar size defined by the NS signal (Fig. 9B1, 9C, and Table 1). The NS-positive nucleolar area (No) and its ratio to the total nuclear area (No/Nu) in the siRSL1D1-treated cells were 35.0 (±1.2, in 100 pixels) and 14.1% (±0.4), compared to the 42.4 (±1.3, in 100 pixels) and 16.8% (±0.4) in the siNEG-treated cells ($p<0.001$, n=130). Although the siRSL1D1 treatment produced a slight and statistically insignificant increase in the NS intensity in the nucleolus relative to its nucleoplasmic intensity (N/P) ($p=0.09$), the overall immunofluorescence of NS in the nucleolus (NoxN/P) was still decreased by the RSL1D1 knockdown ($p=0.05$). No difference was seen in the total nuclear area and the number of nucleolus per cells between the siRSL1D1-treated and siNEG-treated samples, indicating that these nucleolar phenotypes were not caused by sampling errors or by changes in the overall cell condition (Table 1). To determine if siRSL1D1 knockdown interfered with other nucleolar proteins, we immunolabeled B23 in the same sets of cells stained with anti-NS antibody. Our analyses showed that siRSL1D1 could also reduce the nucleolar occupancy of B23, measured by the size of the nucleolus, the ratio between the nucleolar and nuclear size, and the total fluorescence in the nucleolus (Fig. 9B2, 9C, and Table 1). Together, these results show that a partial loss of RSL1D1 expression reduces the amount of NS and B23 in the nucleolus.

Discussion

This study is designed to understand the mechanism that regulates the partitioning of NS between the nucleolus and the nucleoplasm. Our data reveal a complex model that involves nucleolar and nucleoplasmic components, as well as distinct domains of NS (Fig. 10). The nucleolar localization of NS is mediated by its B- and G-domains, and blocked by its I-domain. This I-domain-mediated nucleoplasmic-retaining mechanism does not depend on the B- or the G-domain, but is disabled by the GTP-bound G-domain. Without the I-domain,

the G-domain is localized in the nucleolus regardless of its GTP-binding state. NS interacts with an L1-domain-containing gene, RSL1D1, identified by a yeast two-hybrid screen. NS and RSL1D1 co-localize with each other in the same subnucleolar compartment. The interaction between these two proteins requires the B- and G-domains of NS on one hand and a non-nucleolar, non-L1-domain-containing region of RSL1D1 (a.a. 317–452) on the other hand. Overexpression of a nucleolar RSL1D1 mutant lacking the NS-binding ability (nlsL1) disperses the NS signal from the nucleolus. A partial loss of RSL1D1 expression reduces mostly the compartmental size but also the protein amount of NS in the nucleolus.

The B-domain and the G-domain of NS display two distinctively different nucleolar retention properties. It is unclear why two domains with different retention kinetics are needed for the nucleolar localization of NS. One possibility is that the short retention signal (the B-domain) is used to fine tune the long retention signal (the G-domain). When both domains are present (NSdA), its FRAP signal becomes less than that of the GI-domain only during the very late phase of the recovery (Fig. 1C3). Another possibility is that the B-domain and the G-domain may take part in different biological activities coordinated by NS. At the molecular level, we are unable to distinguish the B- and the G-domain by their interacting partners as yet. Both domains bind the same nucleolar protein, RSL1D1. Notably, the interaction between the G-domain and RSL1D1 also requires the N-terminal 73 amino acids of the I-domain, which contains the G2 and G3 GTP-binding motifs that are less conserved and shorter than the G4 and G1 motifs. To molecularly dissect the different domains of NS and RSL1D1, some truncated mutants are inevitably left without a NLS. Since nuclear translocation is a prerequisite step for initiating nucleolar localization after the protein is synthesized, we used a SV40 NLS to bring those mutant proteins into the nucleus. Although we have shown that this SV40 NLS alone is not sufficient to confer nucleolar distribution (Fig. 1B, nlsHd3), it may still cooperate with and enhance the activity of the NoLS of NS to a different degree when compared to the NLS of NS. This may explain why the G-domain can enter the nucleolus when tagged with an SV40 NLS, but is unable to bind RSL1D1 by itself.

RSL1D1 represents a nucleolar component that regulates the nucleolar localization of NS. At the molecular level, the nucleolus-targeting and RSL1D1-interacting activities of NS are encoded by the same domains, whereas the nucleolus-targeting and NS-binding domains of RSL1D1 are different. At the functional level, the nucleolar retention time of RSL1D1 is longer than that of the full-length NS, and resembles the FRAP recovery kinetics of the GI-domain. Overexpression of a RSL1D1 mutant, nlsL1, can disperse the NS signal from the nucleolus. Since the nucleolar nlsL1 cannot bind NS, this mutant may occupy the nucleolar binding sites for endogenous RSL1D1, and functions as a dominant negative regulator for the nucleolar NS. A partial loss of RSL1D1 expression reduces the NS-defined nucleolar size by 18%. Although the NS signal intensity in the nucleolus appeared elevated, the overall NS fluorescence signal in the nucleolus of siRSL1D1-treated cells was still reduced by 10% compared to the siNEG-treated cells (p=0.05). The changes in the NS distribution associated with the siRSL1D1 treatment are mild, which may be due to an incomplete knockdown effect. It is difficult to assess the efficiency of siRSL1D1 treatment at the endogenous protein level without an anti-RSL1D1 antibody. Notably, the siRSL1D1 treatment also reduces the nucleolar distribution of B23, suggesting that RSL1D1 may directly regulate the nucleolar distribution of B23, or may affect B23 indirectly through NS. This finding also indicates that the nucleolus is composed of different compartments that are interconnected with one another. Together, these results support the in vivo importance of RSL1D1 in regulating the nucleolar localization of NS.

Given the role of RSL1D1 in the nucleolar distribution of NS and that RSL1D1 cannot bind the GTP-unbound GI mutant (GI(256), Fig. 6C), the timing of the dissociation between NS

and RSL1D1, as well as the nucleolar exit of NS, may be triggered by the GTP hydrolysis of NS. GTP hydrolysis is a tightly regulated biological event for all GTP-binding proteins. NS belongs to a subfamily of GTPases containing a MMR_HSR1 domain in the pfam database. Unlike the *ras* protein, all members in this subfamily have four GTP-binding motifs arranged in a circularly permuted order, where the G4 motif is localized N-terminally to the G1, G2, and G3 motifs (Daigle et al., 2002;Leipe et al., 2002). To date, only one gene in this family in multicellular organisms has been experimentally shown to contain some intrinsic GTPase activities (Reynaud et al., 2005). To address if the nucleolar exit of NS is triggered by GTP hydrolysis, we made a Pro 258 to Val mutation on NS, which corresponded to the constitutively active human *ras* protein (H-*ras*(G12V)) in position. However, this NS(P258V) mutant failed to yield a constitutively active phenotype regarding its GTP-binding or nucleolar retention property, indicating that some fundamental differences in the GTP-binding structures exist between the MMR_HSR1 family and the small GTPase family.

The modular property of NS provides a molecular basis for predicting the roles of proteins that interact with different parts of NS. For example, a protein that binds the B- and/or G domains may be mediating the nucleolar targeting/retention step of NS, transported to the nucleolus by NS, or acting downstream of the nucleolar functions of NS. Supporting this idea, we have shown that the B- and G-domain-interacting RSL1D1 is involved in the nucleolar localization of NS. The human homologue of RSL1D1 was previously identified in the gene sets inhibited by cellular senescence (AAN41298), or overexpressed by the non-small-cell lung cancer (AAT06742) and human trophoblast cells (CAA07491). Similarly, NS is highly expressed by several types of human cancer cells (Liu et al., 2004; Tsai and McKay, 2002), and its expression is suppressed in mouse embryonic fibroblast cells undergoing cellular senescence (Zhu et al., 2006). RSL1D1 displays a wider distribution than NS during embryogenesis and in adult mice. The fact that some tissues express RSL1D1 but not NS suggests that it may also work as a nucleolar hub for proteins other than NS. Proteins interacting with the I-domain remain unidentified at this moment. They are expected to serve as the nucleoplasmic docking sites for NS. The nucleoplasmic-retaining activity of the I-domain does not depend on the B- or G-domains, suggesting that it can be used by other nucleolar proteins. A blast search of the Genebank database identifies only two protein sequences that share significant homologies with the I-domain of NS. They belong to the GNL3L (guanine nucleotide binding protein 3-like) and Ngp1 genes, which represent the closest family members for NS in vertebrates. It will be interesting to see if those nucleoplasmic docking sites, once identified, are free-floating or tethered to the nuclear matrix, and if all NS family genes share the same docking molecule.

In conclusion, we show that the dynamic distribution of NS between the nucleolus and the nucleoplasm is controlled by a combination of nucleolar and nucleoplasmic mechanisms. This work raises the idea that the partitioning of nucleolar proteins between subnuclear compartments employs complex molecular devices to achieve a specific, rapid, and reversible response.

Materials and Methods

Recombinant plasmids and site-directed mutagenesis

Deletions and point mutations were introduced by the stitching PCR method as described previously (Tsai and McKay, 2002; Tsai and McKay, 2005). The final PCR products were subcloned into pCIS expression vectors and confirmed by sequencing. Full-length RSL1D1 cDNAs were cloned from mouse embryonic stem cells and human MCF7 cells by reverse transcription-PCR.

Cell culture, transfection, and immunostaining

Three different cell lines, which all expressed NS, were used in this study. HEK293 cells were used for biochemical studies because of their high transfection efficiency and protein production. U2OS cells were used for subcellular distribution analysis because of their large and flat-shaped nuclei. CHO cells were used for the FRAP experiments because of their simple nucleolar morphology. Cells were maintained in Dulbecco's modified Eagle's medium supplemented with 5% fetal bovine serum (Hyclone), penicillin (50 IU/ml), streptomycin (50ug/ml), and glutamine (1%). Plasmid transfections were performed using a standard calcium phosphate method for HEK293 cells or Lipofectamine-Plus reagents (Invitrogen) for U2OS cells, and analyzed 2 days after transfection. Immunofluorescence studies were performed as described previously (Tsai and McKay, 2005). Cells were fixed with fresh 4% paraformaldehyde on ice for 15 minutes. Primary antibodies included: affinity-purified polyclonal Ab2438 (1:500X; chicken IgY) for endogenous NS, monoclonal anti-HA antibody (1:2000X; HA.11, Covance), monoclonal anti-myc antibody (1:1000X; 9E10, Covance), monoclonal anti-fibrillarin antibody (1:1000X; 38F3, EnCor), and monoclonal anti-B23 antibody (1:1000X, Zymed). Secondary antibodies were conjugated with Red-X or FITC.

Yeast two-hybrid screen

The GTP-binding and intermediate domains (GI) of rat NS (amino acids 106–459) was subcloned in the pAS2-1 vector as a bait to screen a 7-day-old mouse embryo cDNA library in pACT2 (Clontech). The bait and library plasmids were cotransformed into *Saccharomyces cerevisiae* strain Y190 and selected for both histidine$^+$ and β-galactosidase$^+$ phenotypes. cDNA plasmids were shuttled into *Escherichia coli* HB101 by electroporation and determined for their sequences.

Coimmunoprecipitation

Cells were harvested in NTEN buffer (20 mM Tris pH8.0, 150 mM NaCl, 1 mM EDTA, 0.5% NP40, 0.1 mM DTT, supplemented with 1 mM PMSF, 1 ug/ml leupeptin, 0.5 ug/ml aprotinin, 0.7 ug/ml pepstatin A, and 1 uM E64). Lysates were incubated with monoclonal anti-HA (HA.11, Covance), monoclonal anti-myc (9E10, Covance), or polyclonal anti-NS (Ab1164) antibody for 1 hour at 4C, followed by incubation with protein G sepharose beads (Pharmacia) for additional 4 hours at 4C. Immunoprecipitates were washed 5 times with RIPA buffer (1X PBS, 0.1% SDS, 0.5% sodium deoxycholate, 1% NP40, 1 mM PMSF, 1 ug/ml leupeptin, 0.5 ug/ml aprotinin, 0.7 ug/ml pepstatin A, and 1 uM E64), fractionated by 10% sodium dodecyl sulfate-polyacrylamide gel electrophoresis (SDS-PAGE), and transferred to Hybond-P membranes (Amersham). Specific signals were detected by Western blot analyses using polyclonal anti-HA or anti-myc primary antibodies and horseradish peroxidase-conjugated secondary antibodies.

GST pulldown assay

Full-length and partial cDNAs of RSL1D1 and NS were subcloned into the pGEX4T-2 vector. GST fusion proteins were expressed in BL21/DE3 as described previously (Tsai and McKay, 2002). Epitope-tagged proteins were expressed in HEK293 cells and extracted in phosphate-buffered saline (PBS)-Triton X-100 (1%) buffer, supplemented with protease inhibitors. Sepharose-bound GST fusion proteins (2 ug) were incubated with cell lysates for 2 hours at 4C, washed five times with extraction buffer, including two times with high-salt solutions (500 mM NaCl), fractionated on 10% SDS-PAGE, and detected by Western blottings.

Northern blot analyses

Ten micrograms of total RNAs were isolated from CD-1 mice using Trizol solutions (Invitrogen), fractionated on a 1% formamide denaturing agarose gel, and transferred onto Hybond XL membrane (Amersham). Filters were then hybridized with α-^{32}P-labeled probes at 65C overnight and washed with high stringency. Plaque date was counted as embryonic day 0.5 (E0.5).

Small RNAi knockdown

siRNA duplexes were designed to target the sense sequence 5′-AGT GGT TCT TGC AGT GCT A-3′ in the human RSL1D1 gene and a scrambled sequence 5′-TGA CGA TCA GAA TGC GAC T-3′ (Dharmacon). Cells were transfected with siRNA duplexes (100nM) for 15 hours using the Oligofectamine reagent (Invitrogen), and fixed with 4% paraformaldehyde 3 days after transfection. The distributions of endogenous NS and B23 were detected by anti-NS (Ab2438) and anti-B23 immunofluorescence, and counterstained with DAPI.

FRAP analysis

CHO cells grown in Nalgene Lab Tek II chamber slides were transfected with 0.6μg plasmid DNA using Lipofectamine-Plus reagents one day before the measurement. Bleaching experiments were performed on a Zeiss LSM510 confocal microscope with a 63X plan-apochromat oil objective. The photobleaching protocol was modified based on previous reports (Dundr et al., 2000; Phair and Misteli, 2000). The GFP signal was excited with the 488 nm Argon laser (20 mW nominal output), and emission was monitored above 505 nm. Cells were maintained at 35C with a heat blower throughout the entire procedure. A spot of 1 um in diameter was bleached within the nucleolus using a short laser pulse administered at 100% power for three iterations. All experiments were ensured to achieve 70–80% bleaching of the original intensity. For image acquisition, the laser power was attenuated to 0.6% of the bleach intensity, and cells were scanned with 5X zoom at 0.29-second intervals for 31.6 seconds after photobleaching. For quantification, fluorescence intensities of the region of interest, the entire nucleus, and outside of the nucleus were measured. Signal recovery in the bleached area (FRAP) was normalized to the total intensity in the nucleus after background subtraction and averaged over 20 cells from three independent experiments. Cells with signal loss more than 10% during the imaging phase were not used.

Image acquisition and analyses

Confocal images were captured on a Zeiss LSM510 confocal microscope using a 63X plan-apochromat oil objective. In Fig. 2, images were scanned with a 512x512 frame size, 2X zoom, and <1.4 um optical thickness. For high-resolution studies (Fig. 4, Fig. 8, and Fig. S2), images were scanned with a 512x512 frame size and 4X zoom. Optical slices of 0.7 um were sampled by setting the pinhole size at less than 1 Airy Unit. Detector gain and amplifier offset were adjusted to ensure all signals were appropriately displayed within the linear range. Immunofluorescent images were captured on a Zeiss Axiovert 200 microscope using a 63X plan-apochromat oil objective and a CoolSNAP*EZ* Monochrome camera (Photometrics, 6.45 × 6.45-um pixels). Exposure time was set so that the brightest intensity reached 80% of the saturation intensity. For the siRNA experiments, captured images were analyzed using the ImageJ 1.36b software (http://rsb.info.nih.gov/ij/). The nucleolar size, the ratio of nucleolar-to-nuclear area, and the ratio of nucleolar-to-nucleoplasmic (N/P) fluorescence intensity were measured from 130 cells randomly sampled from 7 independent experiments in a double-blind way. All nucleolar regions within a single cell were delineated. The average intensities of the whole nucleolar and nucleoplasmic areas were calculated to generate the N/P intensity ratio. Areas were measured in pixels (100 pixels = 0.89 um^2).

Supplementary Material

Refer to Web version on PubMed Central for supplementary material.

Acknowledgments

We thank Seokwoon Kim and Qubo Zhu for their technical support of this work. This project is supported by TIRR/Mission Connect startup fund and R01 CA113750-01 to R.Y.T.

References

Andersen JS, Lam YW, Leung AK, Ong SE, Lyon CE, Lamond AI, Mann M. Nucleolar proteome dynamics. Nature 2005;433:77–83. [PubMed: 15635413]

Baddoo M, Hill K, Wilkinson R, Gaupp D, Hughes C, Kopen GC, Phinney DG. Characterization of mesenchymal stem cells isolated from murine bone marrow by negative selection. J Cell Biochem 2003;89:1235–1249. [PubMed: 12898521]

Bernardi R, Scaglioni PP, Bergmann S, Horn HF, Vousden KH, Pandolfi PP. PML regulates p53 stability by sequestering Mdm2 to the nucleolus. Nat Cell Biol 2004;6:665–672. [PubMed: 15195100]

Carmo-Fonseca M, Mendes-Soares L, Campos I. To be or not to be in the nucleolus. Nat Cell Biol 2000;2:E107–112. [PubMed: 10854340]

Chen D, Huang S. Nucleolar components involved in ribosome biogenesis cycle between the nucleolus and nucleoplasm in interphase cells. J Cell Biol 2001;153:169–176. [PubMed: 11285283]

Daigle DM, Rossi L, Berghuis AM, Aravind L, Koonin EV, Brown ED. YjeQ, an essential, conserved, uncharacterized protein from Escherichia coli, is an unusual GTPase with circularly permuted G-motifs and marked burst kinetics. Biochemistry 2002;41:11109–11117. [PubMed: 12220175]

Dundr M, Misteli T, Olson MO. The dynamics of postmitotic reassembly of the nucleolus. J Cell Biol 2000;150:433–446. [PubMed: 10931858]

Fox AH, Lam YW, Leung AK, Lyon CE, Andersen J, Mann M, Lamond AI. Paraspeckles: a novel nuclear domain. Curr Biol 2002;12:13–25. [PubMed: 11790299]

Leipe DD, Wolf YI, Koonin EV, Aravind L. Classification and evolution of P-loop GTPases and related ATPases. J Mol Biol 2002;317:41–72. [PubMed: 11916378]

Liu SJ, Cai ZW, Liu YJ, Dong MY, Sun LQ, Hu GF, Wei YY, Lao WD. Role of nucleostemin in growth regulation of gastric cancer, liver cancer and other malignancies. World J Gastroenterol 2004;10:1246–1249. [PubMed: 15112336]

Martel C, Macchi P, Furic L, Kiebler MA, Desgroseillers L. Staufen1 is imported into the nucleolus via a bipartite nuclear localization signal and several modulatory determinants. Biochem J 2006;393:245–254. [PubMed: 16162096]

Mekhail K, Gunaratnam L, Bonicalzi ME, Lee S. HIF activation by pH-dependent nucleolar sequestration of VHL. Nat Cell Biol 2004;6:642–647. [PubMed: 15181450]

Mekhail K, Khacho M, Carrigan A, Hache RR, Gunaratnam L, Lee S. Regulation of ubiquitin ligase dynamics by the nucleolus. J Cell Biol 2005;170:733–744. [PubMed: 16129783]

Misteli T. Going in GTP cycles in the nucleolus. J Cell Biol 2005;168:177–178. [PubMed: 15657389]

Olson MO, Dundr M. The moving parts of the nucleolus. Histochem Cell Biol 2005;123:203–216. [PubMed: 15742198]

Pederson T. The plurifunctional nucleolus. Nucleic Acids Res 1998;26:3871–3876. [PubMed: 9705492]

Phair RD, Misteli T. High mobility of proteins in the mammalian cell nucleus. Nature 2000;404:604–609. [PubMed: 10766243]

Politz JC, Lewandowski LB, Pederson T. Signal recognition particle RNA localization within the nucleolus differs from the classical sites of ribosome synthesis. J Cell Biol 2002;159:411–418. [PubMed: 12427865]

Politz JC, Polena I, Trask I, Bazett-Jones DP, Pederson T. A nonribosomal landscape in the nucleolus revealed by the stem cell protein nucleostemin. Mol Biol Cell 2005;16:3401–3410. [PubMed: 15857956]

Reed ML, Dove BK, Jackson RM, Collins R, Brooks G, Hiscox JA. Delineation and modelling of a nucleolar retention signal in the coronavirus nucleocapsid protein. Traffic 2006;7:833–848. [PubMed: 16734668]

Reynaud EG, Andrade MA, Bonneau F, Ly TB, Knop M, Scheffzek K, Pepperkok R. Human Lsg1 defines a family of essential GTPases that correlates with the evolution of compartmentalization. BMC Biol 2005;3:21. [PubMed: 16209721]

Rubbi CP, Milner J. Non-activated p53 co-localizes with sites of transcription within both the nucleoplasm and the nucleolus. Oncogene 2000;19:85–96. [PubMed: 10644983]

Rubbi CP, Milner J. Disruption of the nucleolus mediates stabilization of p53 in response to DNA damage and other stresses. Embo J 2003;22:6068–6077. [PubMed: 14609953]

Sheng Z, Lewis JA, Chirico WJ. Nuclear and nucleolar localization of 18-kDa fibroblast growth factor-2 is controlled by C-terminal signals. J Biol Chem 2004;279:40153–40160. [PubMed: 15247275]

Sleeman JE, Trinkle-Mulcahy L, Prescott AR, Ogg SC, Lamond AI. Cajal body proteins SMN and Coilin show differential dynamic behaviour in vivo. J Cell Sci 2003;116:2039–2050. [PubMed: 12679382]

Tsai RY. A molecular view of stem cell and cancer cell self-renewal. Int J Biochem Cell Biol 2004;36:684–694. [PubMed: 15010332]

Tsai RY, McKay RD. A nucleolar mechanism controlling cell proliferation in stem cells and cancer cells. Genes Dev 2002;16:2991–3003. [PubMed: 12464630]

Tsai RY, McKay RD. A multistep, GTP-driven mechanism controlling the dynamic cycling of nucleostemin. J Cell Biol 2005;168:179–184. [PubMed: 15657390]

Weber JD, Taylor LJ, Roussel MF, Sherr CJ, Bar-Sagi D. Nucleolar Arf sequesters Mdm2 and activates p53. Nat Cell Biol 1999;1:20–26. [PubMed: 10559859]

Wong JM, Kusdra L, Collins K. Subnuclear shuttling of human telomerase induced by transformation and DNA damage. Nat Cell Biol 2002;4:731–736. [PubMed: 12198499]

You J, Dove BK, Enjuanes L, DeDiego ML, Alvarez E, Howell G, Heinen P, Zambon M, Hiscox JA. Subcellular localization of the severe acute respiratory syndrome coronavirus nucleocapsid protein. J Gen Virol 2005;86:3303–3310. [PubMed: 16298975]

Zhu Q, Yasumoto H, Tsai RY. Nucleostemin delays cellular senescence and negatively regulates TRF1 protein stability. Mol Cell Biol. 2006 (in press).

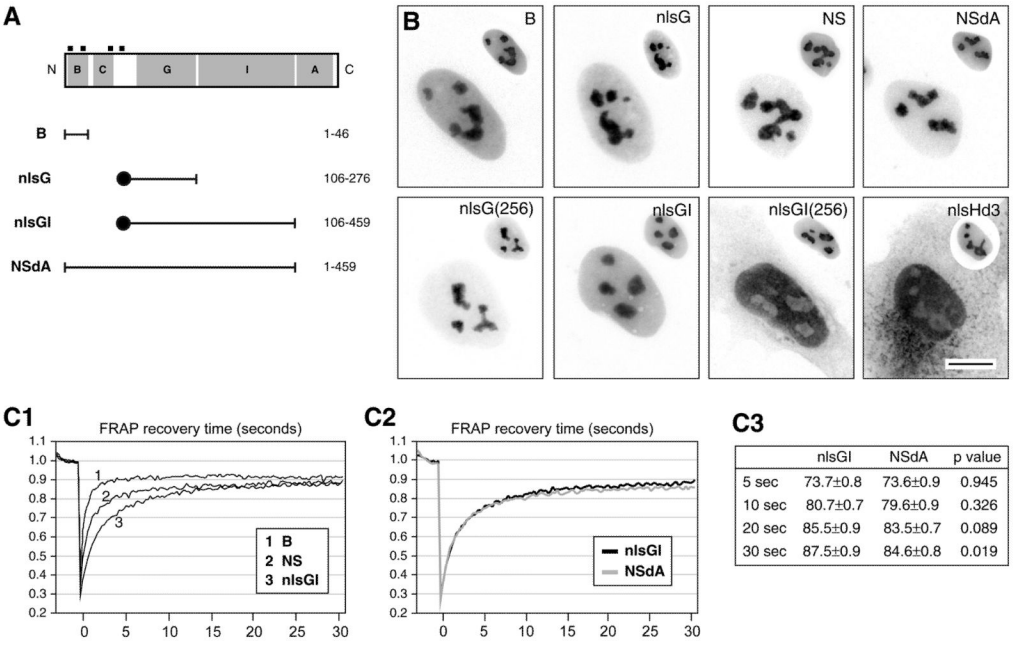

	nlsGI	NSdA	p value
5 sec	73.7±0.8	73.6±0.9	0.945
10 sec	80.7±0.7	79.6±0.9	0.326
20 sec	85.5±0.9	83.5±0.7	0.089
30 sec	87.5±0.9	84.6±0.8	0.019

Figure 1. Nucleostemin (NS) contained two distinct nucleolus-targeting regions with different nucleolar retention time

(**A**) A schematic diagram of NS protein structure and mutant constructs used to determine the nucleolus-targeting domains of NS. An SV40 nuclear localization signal (NLS, black circle) was engineered in mutants missing the endogenous NLS (black boxes). Numbers indicate the amino acid positions. Abbreviations: B, basic; C, coiled-coil; G, GTP-binding; I, intermediate; A, acidic. (**B**) The subcellular distributions of mutant proteins in U2OS cells were revealed by a C-terminal green fluorescent protein (GFP) tag, and counterstained with anti-B23 immunofluorescence shown in the right upper quadrants on a 50% scale. Both the B- and the G-domains (nlsG) displayed a nucleolar distribution pattern. A mutation in the conserved GTP-binding residue G256 (nlsG(256)) did not affect the nucleolar localization of the G-domain alone. When the I-domain was present, such a mutation would abolish its nucleolar localization (nlsGI(256)). A cytoplasmic hydrolase protein (Hd3) was tagged with the SV40 NLS to demonstrate that this sequence was not sufficient to confer nucleolar localization. Scale bar: 10 um. (**C1**) The FRAP (fluorescence recovery after photobleaching) recovery time (X-axis, in seconds) of the B-domain (trace 1), the full-length NS (trace 2), and the GI-domain (trace 3) was determined in Chinese hamster ovary (CHO) cells transiently transfected with the GFP-fusion constructs. The Y-axis represented the percentage of the fluorescence intensity in the bleached area relative to the prebleached intensity. (**C2**) The FRAP recovery time of the GI-domain (nlsGI) and the A-domain deletion mutant (NSdA) was measured as described in the methods section. Statistical analyses at 5, 10, 20, and 30 seconds were shown in (**C3**) (mean ± standard error of mean *(s.e.m)*, n=20).

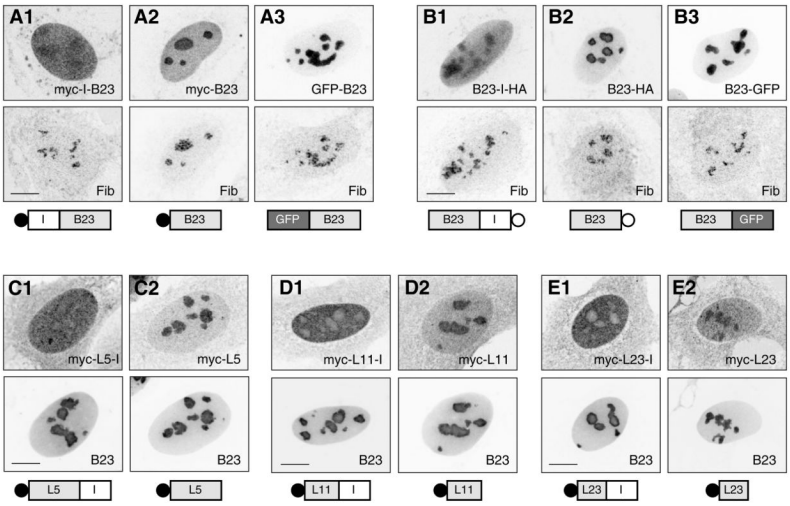

Figure 2. The nucleolar localization of NS was gated by a nucleoplasmic-retaining mechanism independent of its nucleolus-targeting domains

When fused to the N-terminus (**A1**) or the C-terminus (**B1**) of B23, the I-domain of NS significantly increased the amount of B23 in the nucleoplasm, compared to the epitope-tagged (**A2**, **B2**) or the GFP-tagged proteins (**A3**, **B3**) at their respective ends. This nucleoplasmic-retaining activity of the I-domain could also be transferred to three ribosomal proteins, L5, L11, and L23. Unlike the nucleolar distributions of their original proteins (**C2**, **D2**, **E2**), the I-domain fusions of these proteins (**C1**, **D1**, **E1**) were localized almost exclusively in the nucleoplasm. Anti-fibrillarin or anti-B23 immunostainings of the same cells were shown in the bottom panels. Fusion constructs were depicted at the bottom of each panel. Scale bar: 10 um.

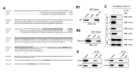

Figure 3. NS interacted with a ribosomal L1 domain-containing protein 1, RSL1D1

(**A**) Protein sequences of mouse RSL1D1 (NM_025546) and two closely related genes, L10A (NM_011287), and L10 (XM_138143), were aligned by the Clustal W (1.81) program. The shaded and underlined areas represented the ribosomal L1 and the coiled-coil domain, respectively. Three putative NLS were marked in bold letters. Consensus keys: fully conserved residues, asterisk; conservation of strong groups, double dots; conservation of weak groups, single dot. Biochemical interaction between NS and RSL1D1 was shown by affinity binding assays using GST fusion of RSL1D1 to pull down HA-tagged NS (**B1**) or GST fusion of NS to pull down HA-tagged RSL1D1 (**B2**). (**C**) The NS-RSL1D1 interaction was confirmed by coimmunoprecipitation in both directions. HEK293 cells were cotransfected with HA-tagged NS and myc-tagged RSL1D1 and immunoprecipitated with anti-myc antibody (1st and 2nd rows, left column), anti-HA antibody (3rd and 4th rows, left column), or mouse IgG (1st to 4th rows, right column). The co-purified proteins (1st and 3rd rows) and the immunoprecipitates (2nd and 4th rows) were detected by immunoblotting with the indicated polyclonal antibodies. (**D**) Myc-tagged RSL1D1 could be co-purified with endogenous NS in HEK293 cells by α-NS antiserum (Ab1164), but not by preimmune serum (Cntrl) (left panel). Endogenous NS could also be co-purified with myc-tagged RSL1D1 by α-myc antibody, but not by mouse IgG (right panel).

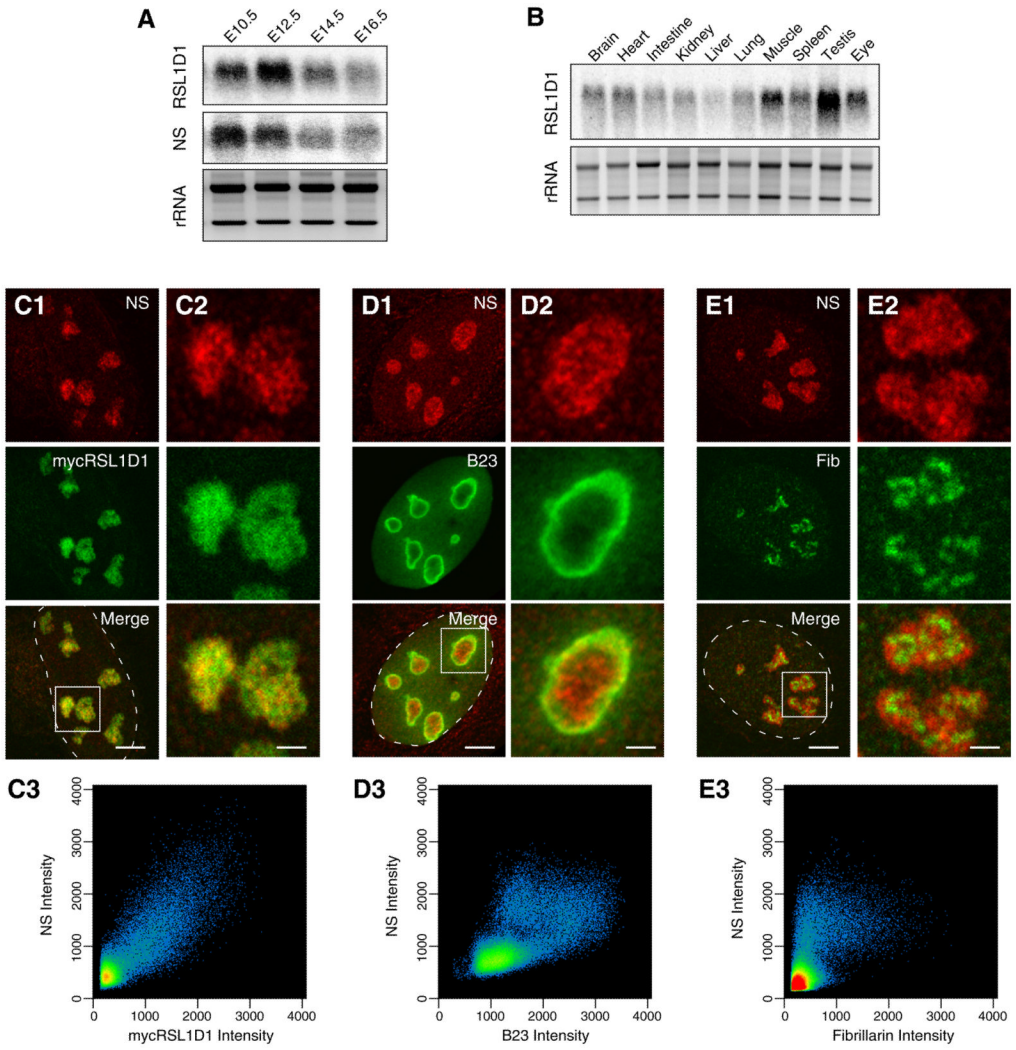

Figure 4. Tissue and subcellular distributions of RSL1D1 overlapped with those of NS

The expression patterns of RSL1D1 and NS in the developing whole embryos from embryonic day 10.5 (E10.5) to E16.5 (**A**) and in the adult mice (**B**) were shown by Northern blot analyses. Colocalization of endogenous NS (red, detected by Ab2438) and myc-tagged RSL1D1 (green), NS (red) and B23 (green), and NS (red) and fibrillarin (green, Fib) were shown by double-labeled immunofluorescence and confocal analyses in (**C**), (**D**), and (**E**), respectively. High magnifications of the indicated areas (squares) were shown in (**C2**, **D2**, and **E2**). Colocalization was quantified in (**C3**, **D3**, and **E3**) where all pixels were plotted based on their red (X-axis) and green (Y-axis) fluorescence intensities, and pseudocolored based on the event frequency, with red representing the highest and blue representing the lowest event frequency. Dashed lines delineate the nucleo-cytoplasmic boundaries. Scale bars: 5 um for C1, D1, and E1; 2 um for C2, D2, and E2.

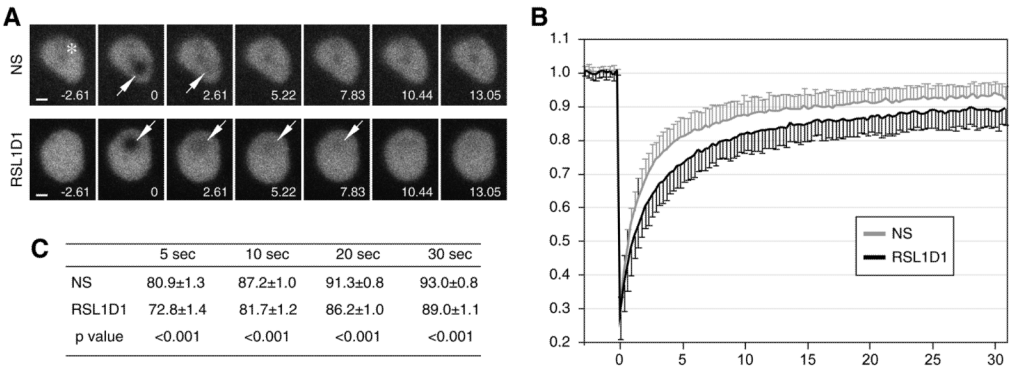

C

	5 sec	10 sec	20 sec	30 sec
NS	80.9±1.3	87.2±1.0	91.3±0.8	93.0±0.8
RSL1D1	72.8±1.4	81.7±1.2	86.2±1.0	89.0±1.1
p value	<0.001	<0.001	<0.001	<0.001

Figure 5. RSL1D1 had a longer nucleolar retention time than NS

(**A**) Time-sequenced FRAP images of NS and RSL1D1 in the nucleolus. A circle of 1um in diameter within the nucleolus (marked by arrows) was bleached. Of note, low intensity spots in the upper panels (indicated by asterisk) existed before photobleaching. Numbers indicate time (in seconds) after the bleaching event. Scale bar: 1 um. (**B**) The FRAP recovery curves of RSL1D1 and NS depicted the average of the fluorescence recovery level (Y-axis, n=20) relative to the prebleached intensity (set as 1) over a 31.6-second period following photobleaching (X-axis, in seconds). Y-error bars represented standard deviations (s.d.) and were omitted on the top and bottom side of the RSL1D1 and NS recovery curves for clarity. (**C**) T-test analyses of the FRAP results were conducted at 5, 10, 20, and 30 seconds after photobleaching (*means* ± *s.e.m*, n=20).

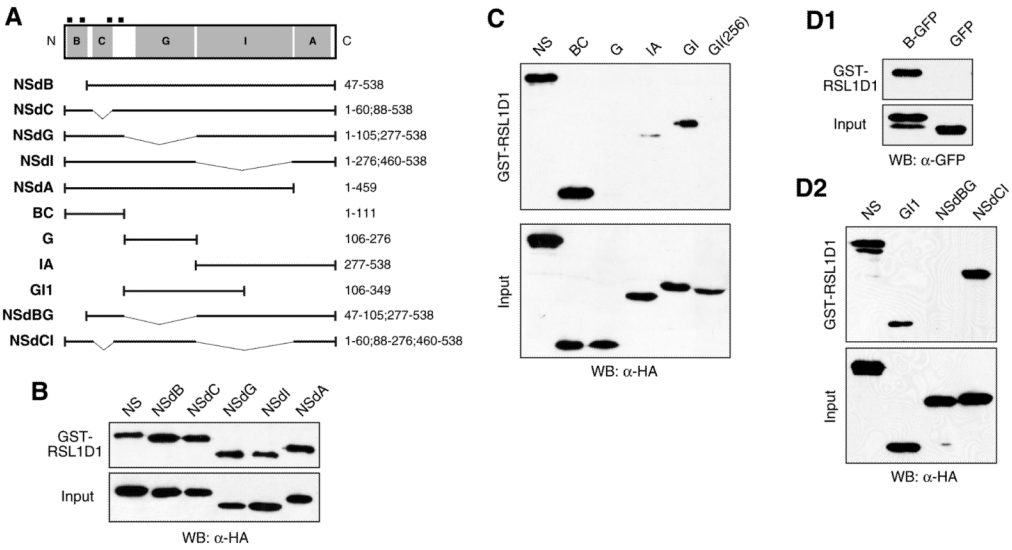

Figure 6. RSL1D1 interacted with the B- and G-domains of NS

(**A**) Schematic diagrams of NS truncated mutants used to determine its RSL1D1-interacting domain(s). (**B**) Affinity binding assays showed that GST fusions of RSL1D1 were able to pull down all single-domain deletion mutants of NS, suggesting that multiple regions were involved. (**C**) Using complex deletion mutants, we showed that RSL1D1 was able to bind both the BC- and the GI-domains, but noy the G-, IA-, or GI-domains with a G256V mutation (GI(256)). The RSL1D1-binding domains of NS were further defined to the B-region of the BC-domain (**D1**) and the GI1-region of the GI-domain (**D2**). (**D2**) Double deletion mutants (NSdBG and NSdCI) confirmed the importance of the B- and G-domains, but not the C- and I-domains, in mediating the NS-RSL1D1 interaction.

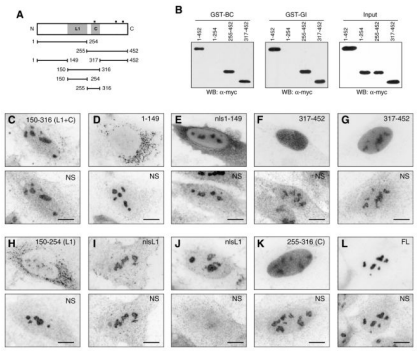

Figure 7. The nucleolar distribution and the NS-interaction of RSL1D1 were controlled by separate domains

(**A**) RSL1D1 contained an L1 domain (amino acid 150–254), a coiled-coil domain (C), and three putative NLS (black boxes). Myc-tagged RSL1D1 truncated mutants were generated to map its NS-interacting and nucleolus-targeting regions. (**B**) Affinity binding assays showed that GST fusions of both the BC- and GI-domains could bind the (317–452) portion of RSL1D1, which did not contain the L1- or C-domain. (**C**-**L**) Anti-myc and anti-NS (Ab2438) double-labeled immunofluorescence demonstrated that the 150–316 region of RSL1D1 was localized in the nucleolus (**C**). The N-terminal 1–149 region was cytoplasmic by itself (**D**), and became partially nucleolar when tagged with an SV40 NLS (**E**). The distribution of the C-terminal 317–452 region was diffuse in the nucleus (**F**), with some cells showing more signals in the nucleolus than in the nucleoplasm (**G**). Within the 150–316 segment, the L1 domain (150–254) was primarily cytoplasmic by itself (**H**), but became mostly nucleolar when provided with a SV40 NLS (**I**, **J**, nlsL1). The coiled-coil domain (255–316) was diffusely localized in the nucleus (**K**). The NS signal was diminished or absent from the nucleolus of many cells expressing nlsL1 (**J**). Scale bar: 10 um.

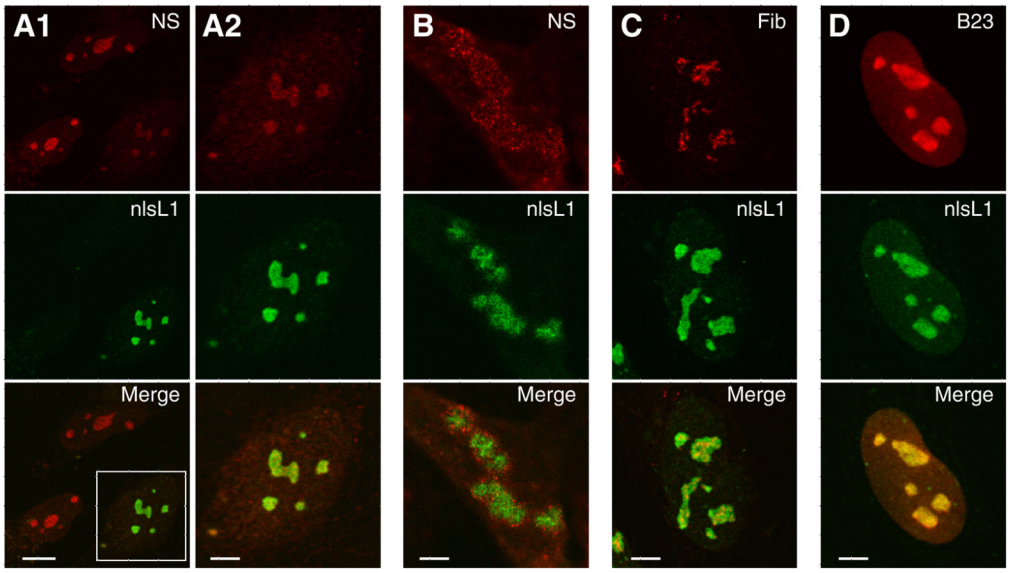

Figure 8. Overexpression of a nucleolar form of the L1-domain (nlsL1) dispersed NS from the nucleolus

(**A1**) The intensities of NS signals in the nucleolus were diminished or disappeared in many cells expressing the nlsL1 mutant. (**A2**) High magnification of the nlsL1-expressing cell showed that its remaining NS signals displayed a reticular pattern of distribution, similar to the NS distribution in wild-type cells. (**B**) In some cells, NS was scattered around the nlsL1 signals. Overexpression of the nlsL1 mutant did not affect the signal intensities or the distribution patterns of fibrillarin (**C**) or B23 (**D**). Scale bars: 10 um for A1; 5 um for A2, B, C, D.

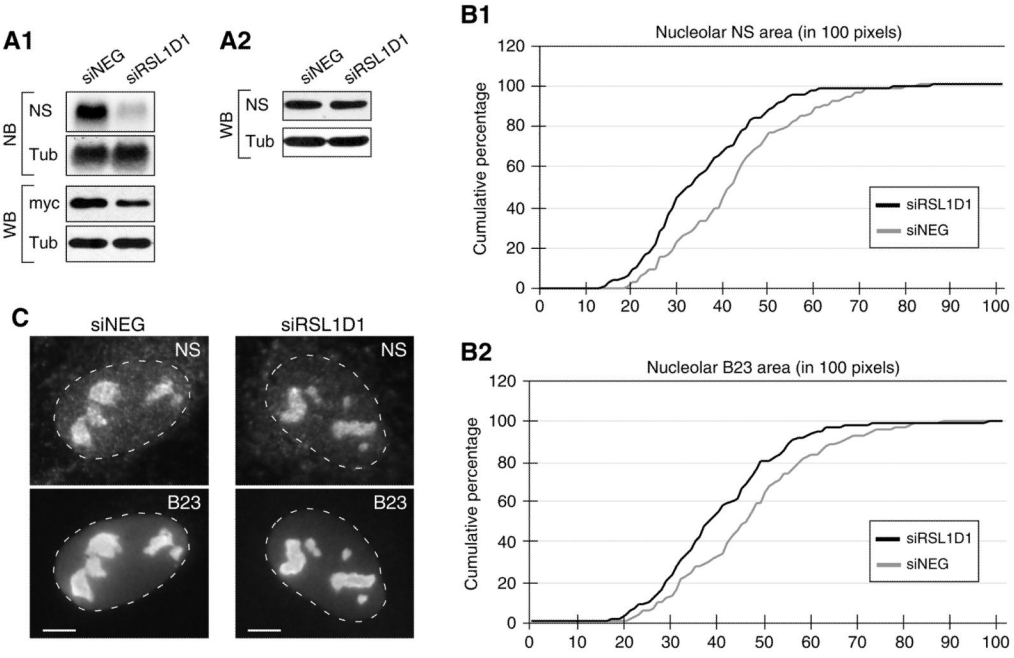

Figure 9. Loss of RSL1D1 expression decreased the compartmental size and protein amount of NS and B23 in the nucleolus

(**A1**) The knockdown efficiency of the RSL1D1-specific siRNA duplex (siRSL1D1) was examined at the RNA and protein levels. Compared to samples treated with the control siRNA duplex (siNEG), siRSL1D1 was able to reduce the endogenous RSL1D1 mRNA by 73% (*top panel*), and the exogenously expressed myc-tagged RSL1D1 protein by 43% in HEK293 cells (*bottom panel*). The siRSL1D1 treatment did not affect the total protein amount of NS (**A2**). Tub: β-tubulin for Northern blots (NB), and α-tubulin for Western blots. The effect of a partial loss of RSL1D1 expression on the nucleolar distribution of NS was measured in U2OS cells double-labeled with anti-NS (Ab2438) and anti-B23 immunofluorescence. Quantitative analyses showed that a partial knockdown of RSL1D1expression decreased the total nucleolar area (No) occupied by NS (**B1**) ($p < 0.001$, n=130). A similar effect was seen in the B23-containing regions (**B2**). The Y-axis represents the percentage of cells at or below the size indicated on the X-axis. The X-axis represents the nucleoluar area in units of 100 pixels (= 0.89 um^2). (**C**) Immunofluorescence images representative of the average of each group were shown. Dashed lines delineate the nucleo-cytoplasmic boundaries. Scale bars: 5 um.

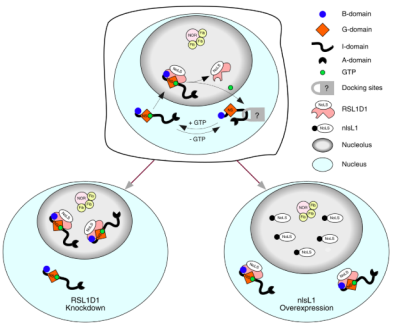

Figure 10. Schematic diagrams of the mechanism controlling NS distribution between the nucleolar and nucleoplasmic compartments, and the effects of RSL1D1 knockdown and nlsL1 overexpression

Our work demonstrates that NS in the GTP-unbound state is blocked from entering the nucleolus by a nucleoplasmic-retaining mechanism that acts on the I-domain. GTP binding releases this lock and allows NS to move into the nucleolus. NS interacts with nucleolar protein RSL1D1 through the nucleolus-targeting B- and G-domains. When not bound by GTP, the GI-domain fails to interact with RSL1D1, suggesting a link between the nucleolar exit of NS and GTP hydrolysis. RSL1D1 co-resides with NS in the same subnucleolar domains surrounding fibrillarin. A partial knockdown of RSL1D1 expression reduces the compartmental size and, to a lesser extent, the protein amount of NS in the nucleolus, supporting with idea that RSL1D1 provides the nucleolar binding site for NS. Overexpression of nlsL1 disperses NS signals from the nucleolus by occupying the nucleolar binding sites for the endogenous RSL1D1 capable of interacting with NS. Symbols for each component were illustrated. Abbreviations: NoLS, nucleolar localization sequence(s); NOR, nucleolar organization region; Fib, fibrillarin.

Table 1

Statistical analyses of FRAP recovery rates of single- and double-residue mutations on NS and GNL3L.

	FRAP recovery percentage		
	T5	**T10**	**T40**
NS	74.0±3.3	84.7±2.4	94.6±2.9
P157F	68.4±4.8 **	76.9±4.4 **	87.6±4.0 **
S178I	79.0±3.0 **	86.7±2.5 **	93.4±3.8
K232A	82.2±2.4 **	89.3±2.0 **	94.8±2.5
F257L	72.9±6.0	79.7±5.6 **	86.8±5.4 **
D1 (P157F-S178I)	77.0±4.4 *	84.6±3.5	91.4±4.2 **
D2 (K232A-F257L)	73.8±4.6	83.1±4.0	91.1±4.1 **
GNL3L	90.2±3.2	94.4±2.6	96.7±3.2
F146P	90.5±1.9	94.6±2.2	97.6±3.0
I168S	89.9±3.8	93.6±2.9	97.4±2.6
A227K	85.5±4.0 **	90.4±2.8 **	96.5±3.0
L254F	89.6±4.1	93.0±4.0	97.7±4.5
K1 (F146P-I168S)	90.0±3.2	93.4±2.8	96.9±2.9
K2 (A227K-L254F)	77.4±8.5 **	84.3±7.6 **	95.3±9.3

Tn FRAP recovery percentage at n seconds

* P-value < 0.01 compared to NS or GNL3L

** P-value < 0.001 compared to NS or GNL3L